# Heavy-ion versus electron-beam excitation of an excimer laser

Thomas J. Moratz, Todd D. Saunders, and Mark J. Kushner[a)]
*Department of Electrical and Computer Engineering, University of Illinois, 1406 West Green Street, Urbana, Illinois 61801*

(Received 15 April 1988; accepted for publication 1 July 1988)

A model is described for the heavy-ion pumping of an XeF($B \rightarrow X$) laser by uranium fission fragments (FF). The model is a self-consistent accounting of the generation and transport of the FF's through the fission foils, slowing of the fragments in the gas, evolution of the secondary-electron-source function and distribution, and the XeF laser plasma kinetics. By simulating the same quantities for an *e*-beam-pumped plasma, direct comparisons can be made for laser performance. We found that the secondary-electron source generated by the *e*-beam is more energetic than that for direct ionization by FF's due to a more favorable mass ratio for momentum transfer collisions with orbital electrons. This difference in the electron-source functions significantly affects $W$ values (energy/ion pair) and excitation fractions. The impact on laser performance, though, is not large due to the high efficiency of channeling deposited energy to the upper laser level in XeF lasers. For conditions typical of FF excitation (power deposition 1–3 kW cm$^{-3}$, pulse length $\approx 200\,\mu$s), *e*-beam excitation results in 10%–15% higher gain than heavy-ion excitation.

## I. INTRODUCTION

Rare-gas halide lasers are being developed as coherent sources of high average and high peak power radiation at ultraviolet wavelengths.[1] Typically, excimer lasers are excited by either electric discharges or electron beams having pulse lengths of less than a microsecond with pump powers of many hundreds of kW cm$^{-3}$ to a few MW cm$^{-3}$.[2] Energy deposition in such systems is typically 50–200 J/$\ell$. New applications of excimer lasers, though, call for pulse lengths exceeding many tens of microseconds. Higher energy deposition over longer pulse lengths is difficult to obtain in discharged excited systems because of issues related to discharge stability.[3] It is also difficult to extend the pulse length and energy deposition in *e*-beam-pumped systems due to heating and subsequent failure of the foil between the *e*-beam diode and laser chamber.

Fission-fragment pumping is an alternate method of exciting gas lasers when long pulse lengths and high-energy deposition are required.[4–7] In this pumping scheme, the laser-gas mixture is contained in a reaction cell lined with a foil impregnated with a fissile material, or the gas mixture itself contains a fissile gas. The reaction cell is placed near a pulsed neutron source which causes fissions in the foil or the gas. The fission fragments, highly charged and energetic ions, impinge on the gas ionizing and exciting the media. Excitation pulse lengths using this method are typically 100 $\mu$s–50 ms, and power deposition is typically tens of W cm$^{-3}$ to a few kW cm$^{-3}$, resulting in energy deposition approaching 500–1000 J/$\ell$.

Fission-fragment (FF) excitation of lasers was first demonstrated in 1975,[8,9] and oscillation has subsequently been obtained on many infrared transitions.[5,6,10,11] Although many schemes have been proposed for fission-fragment excitation of visible and ultraviolet lasers,[12–17] only two visible lasers have been reported.[18,19] The lack of success at obtaining laser oscillation at visible and uv wavelengths is due to the typically shorter lifetimes of the upper laser level at those wavelengths and the higher pump rates required to reach threshold. Recently, though, pulsed neutron sources enabling higher pump rates have become available. Using such a source, a gain at 351 nm of the XeF($B$-$X$) excimer transition has been reported.[20] Although the FF excitation of the XeF($B$-$X$) laser has been previously studied,[17] this successful demonstration has motivated us to reexamine the excitation mechanisms of heavy-ion pumped plasmas and of FF excitation of excimer lasers. As we will show, the excitation processes in *e*-beam and heavy-ion-pumped systems differ, and therefore analogies between the two systems must be carefully made. This condition results from the fact that power deposition is dominated by momentum transfer from the projectile (an electron or heavy ion) to an orbital electron in the target (buffer gas). The difference in mass of the projectile between an *e*-beam and heavy-ion source makes the details of the energy deposition by the two methods quantitatively different.

In this paper, we report on a self-consistent analysis of the heavy-ion excitation of an XeF($B$-$X$) excimer laser using fission fragments and compare those results to electron-beam pumping for the same power deposition. We previously studied excitation of noble gases by energetic heavy ions (a few MeV/amu) by explicitly calculating the slowing of the ions and computing the spectrum of electrons produced by direct ionization of the gas by the fission fragments.[21] We now extend the analysis to include the kinetics of the electrons produced, the resulting excitation rates, and pumping of an XeF($B$-$X$) laser. Analogous rate constants are obtained for electron-beam pumping by using a Monte Carlo simulation for the slowing of a 1-MeV electron beam. By using these values for FF pumping and *e*-beam pumping as input to a plasma chemistry and spectroscopic model for a XeF($B$-$X$) laser, we can compare their respective performances.

In Sec. II, we discuss our models for the fission-frag-

a) Author to whom correspondence should be addressed.

 0021-8979/88/203799-12$02.40  

ment-source function and slowing of the heavy ions. These models provide the electron production term, which is used in a Boltzmann analysis for the electron distribution function, also described in Sec. II. The plasma-chemistry model is described in Sec. III followed by comparisons of $e$-beam and FF pumping of Ne/Xe/$X$ ($X = NF_3, F_2$) gas mixtures in Sec. IV. Implications of these results for exciting XeF($B \rightarrow X$) lasers are discussed in Sec. V, followed by concluding remarks are in Sec. VI.

## II. DESCRIPTION OF THE SOURCE AND SLOWING-DOWN MODELS

In this work, we will examine excitation of Ne/Xe/$F_2$ and Ne/Xe/$NF_3$ gas mixtures by heavy ions resulting from the fission of uranium-impregnated foils lining the walls of a rectangular laser cavity. The method of analysis is as follows. The energy spectrum of fission fragments (FF's) emanating from the foil is first obtained by computing the trajectories of the FF's as they traverse the foil and escape into the gas. The slowing of the FF's as they deposit their energy in the gas is then computed. This is performed by calculating the isotropic velocity distribution of the fragments and convolving the distribution with the pertinent excitation and ionization cross sections to obtain the direct excitation rates and electron-source spectra generated by the fission fragments. The product-electron spectrum resulting from ionizations by the FF's is then used as the influx term in the Boltzmann equation to calculate the product-electron energy distribution. The electron energy distribution, convolved with the appropriate cross sections, yields the electron-impact excitation, ionization, and attachment rate coefficient, as well as the characteristic electron temperature ($T_e = \frac{2}{3}\langle\epsilon\rangle$). In doing so, we can separate contributions to excitation by the fission fragments from those by the product electrons.

Comparisons are made with an electron-beam-pumped system by generating similar electron-impact rate constants using a Monte Carlo simulation for the slowing of a 1-MeV $e$ beam. We make a distinction between the beam electrons and the product secondary electrons to clarify comparisons made to FF's. In this fashion we can compare excitation and ionization events resulting directly from the source projectiles (i.e., the beam electrons and fission fragments) with those resulting from the product electrons. With electron and projectile excitation rates so obtained for $e$-beam and FF pumping, we use them as input to a plasma-chemistry model for an XeF($B$) laser to compare performance.

### A. Fission-fragment-source spectrum

In this section we discuss the spectrum of fission fragments impinging on the laser-gas mixture resulting from the fission of $^{235}U$ in $U_3O_8$ coated foils surrounding the laser cavity. Our procedure is similar to that described by Miley and Theiss,[22] Guyot, Miley, and Verdeyen,[23] and Nguyen and Grossman.[24] It is summarized in the Appendix.

In the neutron-induced fission of $^{235}U$, a distribution of fission fragments are produced. The distribution is approximated by a light particle and a heavy particle, whose characteristics are listed in Table I. The foils are thin enough (3–15 $\mu$m) that there is no attenuation of the neutron flux in traversing the foils. A homogeneous source of fission fragments is therefore generated throughout the foil.

TABLE I. Characteristics of the fission fragments of $^{235}U$.

| | Light fragment | Heavy fragment |
|---|---|---|
| Atomic weight $M$ (amu) | 95 | 139 |
| Atomic number $Z$ | 41 | 57 |
| Fission energy $\epsilon_0$ (MeV) | 99 | 68 |
| (range in foil) × (foil density) $NR$ (cm$^{-2}$) | $1.8\times10^{20}$ | $1.44\times10^{20}$ |

The fission-fragment energy spectrum impinging on the gas, $\varphi(\epsilon)$, is obtained by calculating the probability that the trajectory of a fission fragment starting in the foil reaches the surface with an energy $\epsilon$. The spectrum is normalized so that the total flux of fission fragments, $\Phi$, is given by

$$\Phi = \int_0^\infty \varphi(\epsilon)\, d\epsilon, \tag{1}$$

and the total power deposited in the gas is

$$P = \int_0^\infty \varphi(\epsilon)\epsilon\, d\epsilon. \tag{2}$$

The corresponding FF velocity distribution is $\varphi(V)$.

The FF energy spectra emanating from foils of thicknesses of 3 and 10 $\mu$m are shown in Fig. 1 for the light and heavy fragments. The total range of each fragment in the foil is $\approx 10\,\mu$m. For a given fragment, the high-energy portion of the spectra, $\epsilon > \epsilon^*$ (see the Appendix) is the same for both foils, as this represents the energy above which fragments escape from the foil with trajectories less than the foil thickness. The slope of $\varphi(\epsilon)$ is discontinuous at $\epsilon = \epsilon^*$. Below this energy, fission fragments emerge from the foil after having had trajectories with lengths greater than the foil thickness. Increasing the foil thickness increases the total number of fission events and increases the total number of fission fragments emitted. The additional fragments, though, are emitted from the foil exclusively at low energy, that is with $\epsilon > \epsilon^*$. As the foil thickness increases, the power deposited in the gas reaches a nearly constant value as fission fragments

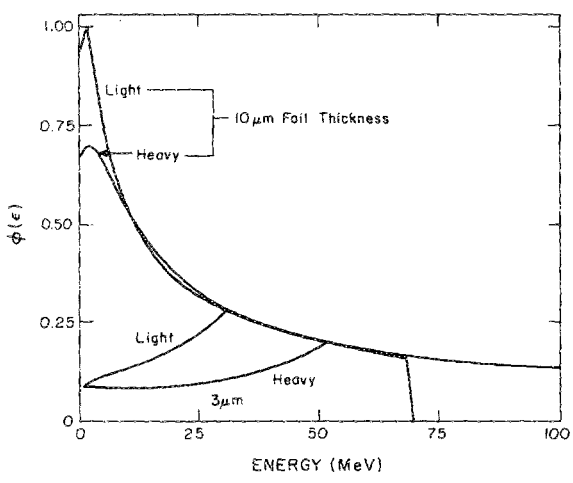


FIG. 1. Energy spectra of light (initial energy 99 MeV) and heavy (initial energy 68 MeV) fission fragments emanating from $U_3O_8$ foils of thickness 3 and 10 $\mu$m. More total fragments are obtained from the thick foil; however, the additional fragments are all exclusively at low energy.

born in the foil at a depth greater than their range do not escape. The optimum foil thickness is approximately 60% of the range of the FF. This is shown in Fig. 2, where power deposited in the gas is plotted as a function of foil thickness. The total flux emitted by the foil, $\Phi$, is also plotted for each fragment. Note that the total power reaches a nearly constant value while $\Phi$ continues to increase. This is a consequence of $\varphi(\epsilon)$ shifting to lower energy as the foil thickness increases. In the results discussed below, we use $\varphi(\epsilon)$ corresponding to a 6-$\mu$m foil.

### B. Fission-fragment velocity distribution

In this section, we describe the method whereby ionization and excitation rates for heavy-ion impact are obtained for the slowing of fission fragments. In doing so, we obtain the spectrum of secondary electrons from direct ionizations by the fission fragments. This spectrum is later used as input to a Boltzmann analysis for the electron distribution function.

The fission fragments, whose flux is initially given by $\varphi(V)$ (see the Appendix), slow with a deceleration given by the electronic stopping power. At low energies, the electronic stopping power is negligibly small, but the FF's still have finite energy. At those energies, the FF's no longer ionize or excite the gas but they do heat the gas. We ignore FF's that slow below this critical energy but self-consistently account for the energy in terms of gas heating in the plasma-chemistry portion of the model.

The first step in computing the slowing of the FF's is to obtain the steady-state, spatially dependent velocity distribution, $F(V,x)$, where $x$ is measured from the surface of the foil. To do so, we use the one-dimensional Boltzmann equation with a deceleration, $S(V)$,

$$-S(V)\frac{\partial F(V,x)}{\partial V}+V\frac{\partial F(V,x)}{\partial x}=0. \tag{3}$$

Integrating over the spatial coordinate and defining $H(V)=\int F(V,x)dx$, we have

$$S(V)\frac{\partial H(V)}{\partial V}=VF(V)\big|_{x=0}^{x}. \tag{4}$$

We extend the integration to where $F$ vanishes. The source spectrum of fission fragments $\varphi(V)$ and velocity distribution $F(V)$ are related by $\varphi(V)=VF(V)$, so

$$H(V)=\int_{v}^{V_{\max}}\frac{\varphi(V)dV}{S(V)}. \tag{5}$$

To obtain the spatially averaged distribution, $\bar{F}(V)$, we divide $H(V)$ by the full fission-fragment range,

$$R(V_{\max})=\int_{0}^{V_{\max}}\frac{V\,dV}{S(V)}$$

$$\Rightarrow\bar{F}(V)=\left(\int_{0}^{V_{\max}}\frac{\varphi(V)dV}{S(V)}\right)\Big/\left(\int_{0}^{V_{\max}}\frac{V\,dV}{S(V)}\right). \tag{6}$$

where $V_{\max}$ is the maximum FF velocity.

The stopping-power formalism of Srivastava and Mukherji[25] is used to obtain the range of the particles. This formalism starts by distinguishing cases with $\chi>1$ and $\chi<1$, where $\chi=2qV_0/V$. Here $q$ is the charge of the fission fragment and $V_0=e^2/\hbar$ ($2.179\times10^8$ cm s$^{-1}$) is the atomic unit of velocity. As the fragments slow down the distribution of charge states is narrow enough that they can be represented with average charge, as given by Betz.[26] For a projectile of nuclear charge $Z_p$, the average charge state is

$$\bar{q}=\frac{1}{2}\frac{V}{V_0}Z_P^{0.45} \tag{7}$$

so that $\chi=Z_P^{0.45}$. For all cases of interest here, $\chi>1$. The distribution of electrons in the target atoms is described by the function

$$f(Z_T)=\begin{cases}Z_T^{1/3}, & Z_T<45,\\ 0.28Z_T^{2/3}, & Z_T>45,\end{cases} \tag{8}$$

where $Z_T$ is the atomic number of the target. For a projectile of mass $M_P$ the stopping power for $V<0.5Z_T\chi^{1/3}V_0$ is given by

$$S(V)=\frac{1}{M_p}\frac{d\epsilon}{dx}$$

$$=\frac{4\pi Ne^4}{M_Pm_e}\left(\frac{q}{V}\right)^2f(Z_T)(3\chi^{-1/3}+\chi^{-1})\frac{V}{V_0}$$

$$=\frac{\pi N\hbar^2}{M_Pm_e}Z_P^{0.9}f(Z_T)(3Z_P^{-0.15}+Z_P^{-0.45})\frac{V}{V_0}, \tag{9}$$

where the velocity corresponding to 1 MeV/amu equals $6.35V_0$. The important result is that $S(V)\sim V$, so that

$$\bar{F}(V)=\frac{1}{V_{\max}}\int\frac{\varphi(V)dV}{V}. \tag{10}$$

In our simulation, we follow the slowing down of both the heavy and light fission fragments, so that at this point we have two velocity distributions.

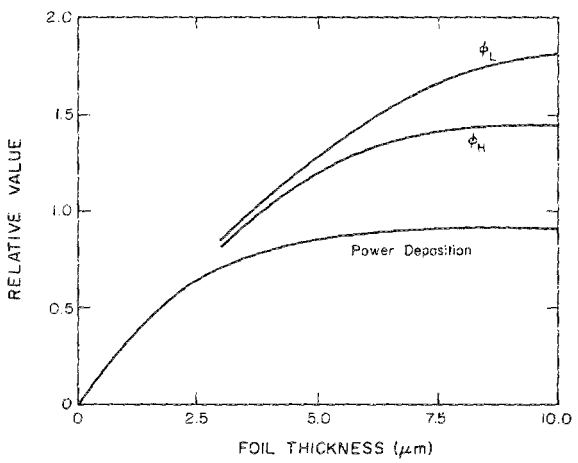


FIG. 2. Relative power deposition into the gas from the fission foil, and the particle fluxes of light and heavy fragments as a function of foil thickness. The power deposition nearly reaches its maximum value at a thickness of 5–6 $\mu$m while the particle fluxes continue to increase, indicating the particles emanate from the foils with decreasing average energy.

### C. Product-electron spectrum

To obtain the spectrum of electrons resulting from direct ionization by the fission fragments we require the differential cross section for ionization, $\sigma_i(V,\epsilon)$, where $V$ is the FF

velocity and $\epsilon$ is the energy of the ejected electron. The spectrum of direct product electrons at energy $\epsilon$, $\psi(\epsilon)$, is then

$$\psi(\epsilon) = N \int_0^\infty \overline{F}(V) V \sigma_i(V,\epsilon) dV, \tag{11}$$

where $N$ is the total gas density.

The binary Coulomb collision cross sections of Gryzinski[27] were used for the transfer of energy from fission fragments to orbital electrons in the gas atoms, as did to Guyot, Miley, and Verdeyen,[23] and Hassan and Deese[28] in their analysis of FF-generated plasmas. Defining $\sigma(V,\Delta\epsilon)$ as the cross section for the transfer of energy $\Delta\epsilon$ to an orbital electron by a FF with velocity $V$, $Q(V,u)$ as the total cross section for a process having threshold energy $u$, and $\Sigma(V,u)$ as the energy-weighted (or stopping power) cross section for all processes with thresholds greater than $u$, we have

$$Q(V,u) = \int_u^U \sigma(V,u')du', \tag{12a}$$

$$\Sigma(V,u) = \int_u^\infty u'\sigma(V,u')du', \tag{12b}$$

$$\sigma_i(V,\epsilon) = \sigma(V,\epsilon + u_i), \tag{12c}$$

where $u_i$ is the ionization potential and $U$ is a specific upper bound (see below). The Gryzinski cross sections have the form

$$\sigma(V,\Delta\epsilon) = \frac{\sigma_0}{(\Delta\epsilon)^3} G\left(\frac{w_i}{\Delta\epsilon}; \frac{V}{v_e}\right), \tag{13}$$

In Eq. (13), $w_i$ is the kinetic energy of the projectile, $v_e$ is the velocity of the orbital electron to which the energy is transferred, and $\sigma_0 = 6.56\times10^{-14}q^2$ cm$^2$ eV$^2$, where $q$ is the charge state of the projectile ion. The function $G$ in Eq. (13) is given in Ref. 27. In using this expression we ignore inner-shell excitations and ionizations. This is a good approximation because the cross section for energy transfer with large $\Delta\epsilon$ is much smaller than that for energy transfer to outer-shell electrons due to the $(\Delta\epsilon)^3$ in the denominator of Eq. (13). The cross sections in Eq. (12) are shown in Fig. 3 for FF collisions and include the effect of the charge state of the ion.

The cross sections described above are for collisions between the fission fragments and a single orbital electron. We therefore need to multiply this cross section by the effective number of orbital electrons per atom that interact with the fission fragments. Previously we used the number of electrons in the outer subshell but found that we could improve upon the result by equating the stopping-power cross section, $\Sigma(V,0)$, with the stopping power, $M_p S(\epsilon)$, and solve for $n_{\text{eff}}$, the effective number of orbital electrons

$$n_{\text{eff}} = M_p S(\epsilon)/M\Sigma(V,0). \tag{14}$$

This value normalizes the cross section and ensures that we conserve energy. The values for $n_{\text{eff}}$ obtained for neon and xenon are shown in Fig. 4 and are approximately half the actual number of outer-shell electrons. At low energy the stopping power is no longer dominated by the electronic stopping power; $\Sigma(V,0)$ vanishes while $S(\epsilon)$ stays finite. To correct for this we set $n_{\text{eff}}$ to a constant value at low energy.

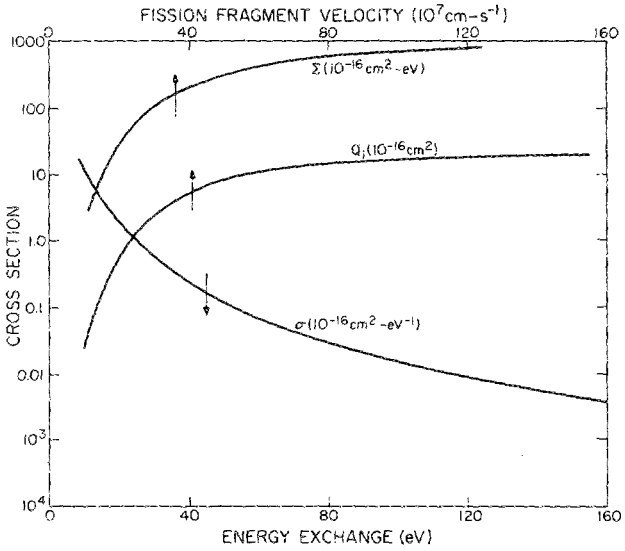


FIG. 3. Fission-fragment collision cross sections in neon given by the Gryzinski formulation weighted by the effective charge of the fission fragment $q(V)$. The differential cross section with respect to energy exchange $\sigma(V,\Delta\epsilon)$ is shown as a function of $\Delta\epsilon$ at an ion velocity of $V^2 = 1$ MeV/amu and the units are Å$^2$/eV. The integral cross section for ionization $Q_i(V)$ (in Å$^2$) is plotted against $V$ (in units of $10^7$ cm/s), as is the stopping power cross section, $\Sigma(V,0)$ (in eV Å$^2$).

This correction has little effect on our results since we require only the rate of electronic excitation, which is negligible at these low energies.

The fact that the collisions by fission fragments result in energy transfer in small increments compared to $e$ beams will be important throughout our discussion. This condition is a consequence of the large ratio ($> 10^5$) of projectile mass (i.e., the fission fragment) to target mass (i.e., an electron) and results in inefficient transfer of kinetic energy. It also produces an effective threshold energy for ionization by FF's at relatively high energy. In neon, the threshold energy for ionization by a heavy particle is approximately 1.7 keV/amu. This large threshold value results in wasted energy with respect to electronic excitation but also allows one to terminate the calculation at a suitably low velocity with no loss of accuracy with respect to electronic energy transfer.

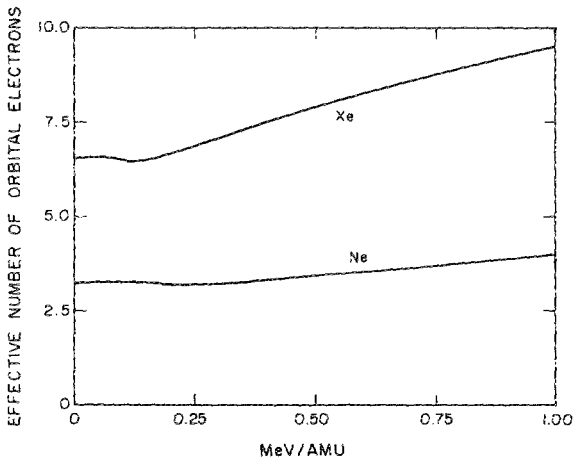


FIG. 4. Effective number of orbital electrons for Xe and Ne for use with Gryzinski cross sections in the heavy-ion slowing-down calculation.

Analogously, had the projectile been an electron, the favorable mass ratio allows much larger incremental energy transfers, resulting in a more energetic electron source spectrum, as discussed below.

### D. Product-electron energy distribution

From the results of the FF slowing down calculation, we obtain the product-electron spectrum, $\psi(\epsilon)$, which is the source of electrons resulting from direct ionization by heavy ions. The product-electron energy distribution, $f(\epsilon)$, is obtained by using the product-electron spectrum as the source term in the solution of Boltzmann's equation. The electron distribution in heavy-ion-generated plasmas has been studied by Lo and Miley,[29] and Hassan and Deese.[28] Those treatments differ in the form of the product-electron spectra. Lo and Miley assumed a $\delta$-function source at 1 keV. Hassan and Deese used an electron-product-source spectrum obtained using binary Coulomb cross sections as we do in this work; however, their ion velocity distribution is fixed as that given by the source function. Our work differs from the work of Hassan and Deese by explicitly calculating the slowing down of the ions.

In the absence of an applied electric field, the spatially averaged Boltzmann equation for $f(\epsilon)$ reduces to

$$\psi(\epsilon) = c\{f(\epsilon)\}, \tag{15}$$

where $C$ is the collision operator representing energy loss by momentum transfer and inelastic collisions. Because of the low excitation fraction of the gas, we can ignore superelastic collisions while including ionization, excitation, and attachment processes. Ionization sources in Boltzmann's equation are handled in the same manner as Yoshida, Phelps, and Pitchford,[30] where the out-scatter term in $C$ uses the total ionization cross section. The in-scatter terms are represented by integrals involving the differential ionization cross sections with respect to the secondary-electron energy. The secondary-electron energy distribution from electron-impact ionization is as given by Opal, Peterson, and Beaty.[31]

In solving Boltzmann's equation, we begin the calculation at the maximum energy of $\psi(\epsilon)$ and compute the down-flux contributing to energies below the current value resulting from inelastic collisions. Two energy grids were used, a coarse grid at energies greater than 100 eV and extending to the maximum energy of $\psi(\epsilon)$, and a fine grid at lower energies, having a resolution of 0.1 eV to better account for threshold behavior and attachment. On the high-energy grid elastic energy losses were ignored, as this contribution to momentum transfer is negligible. The cross sections for excitation and ionization of Ne were obtained from Refs. 32–34, for Xe from Refs. 35 and36, and for $F_2$ from Ref. 37.

### E. *e*-beam slowing-down calculation

Electron-beam pumping of excimer lasers is the conventional method for exciting large volumes (many liters) over moderate pulse lengths (hundreds of ns to a few $\mu$s). For purposes of comparing *e*-beam-pumped systems to heavy-ion-pumped systems, we also computed electron rate coefficients for laser excitation for otherwise identical conditions to that for pumping with FF's (i.e., same pressure, gas mix, and total power deposition). To model the *e*-beam-pumped plasma we used a Monte Carlo particle simulation.

The *e*-beam simulation is a zero (spatial) dimensional version of a model that has been previously described.[38] The beam electrons and beam-produced secondary electrons are tracked in the simulation as they slow down until they are ultimately attached to the halogen donor ($F_2$ or $NF_3$). Relativistic effects in the cross sections were ignored. The secondary-electron distribution of Opal, Peterson, and Beaty[31] was used for ionization.

The beam electrons are started with an energy of 1 MeV. The spectrum of secondary electrons produced by the beam electrons are, from an accounting standpoint, treated independently from the beam electrons. In this way, we separate excitations and ionizations caused directly by the beam electrons from those by the product electrons. In doing so, we can compare results for an *e*-beam-pumped plasma directly with those for a plasma produced by fission fragments.

### F. *W* values for ionization and fractional excitation

The usual method of analysis of *e*-beam-pumped systems is to calculate the electron production or excitation rate in terms of the power deposition using a "$W$" value

$$\frac{\partial n_e}{\partial t} = n_e N k = \frac{P}{W}, \tag{16}$$

where $P$ is the specific power deposition and $W$ is the energy deposition per event, usually quoted in eV. The use of $W$ values for high threshold events (ionization, metastable excitation) is particularly useful for our conditions where the "burn-up" of the halogen may cause large changes in the normalization of the electron energy distribution function, but causes virtually no change in the total rate of these events (see Sec. IV B). This occurs because there is little overlap of cross sections for attachment and high threshold events, and there is no up-flux from an electric field to "mix" electrons sampling these cross sections.

Because of the differences in the electron energy production rates between FF and *e* beams, a fundamental method is required to determine these $W$ values for each method of power deposition. We used our slowing-down calculations to determine these values. In keeping with convention, we calculated a $W$ value for ionization, and expressed the rate of excitation as a fraction of the rate of ionization, $R$. The $W$ values we calculated are for impact ionization of ground-state species only. Other ionization processes, such as Penning ionization and multistep electron-impact ionization, are included in the plasma kinetics portion of the model.

In our notation, the total $W$ value, $W_T$, gives the total electron production rate, and the partial $W$ value for each constituent of the mixture gives the electron production rate for that species. We find that due to competition between species having electron-impact cross sections which overlap, scaling of $W$ values obtained for the pure gases by their mole fractions in a mixture are not accurate. In the absence of superelastic collisions and secondary-electron processes included in the plasma kinetics model, the $W$ values discussed are functions of the gas mixture, FF source function, or *e*-beam energy, but not on the absolute magnitude of the power deposition.

A quantity of interest is the $W$ value for ionization directly by the fission fragments or beam electrons, $W_D$, which ignores ionizations by the product electrons. The direct $W$ value is a measure of the importance of the product electrons in the ionization process; the larger the $W_D$ compared to $W_T$, the more important the product electrons. The ratio of direct to total $W$ value is given by

$$\frac{W_D}{W_T} = 1 + \frac{\text{number of product ionizations}}{\text{number of direct ionizations}}. \quad (17)$$

## III. PLASMA-CHEMISTRY MODEL FOR XeF($B$) EXCITATION

To compare the consequences of the differences in excitation by $e$-beam or FF pumping, a plasma-chemistry model was constructed for an XeF($B$-$X$) laser. The model is an accounting of the electron and heavy-particle kinetics occurring in $Ne/Xe/F_2/NF_3$ gas mixtures. The model uses as input the excitation rates and $W$ values calculated in the manner described above. The electron and heavy-particle reactions used in the plasma-chemistry model are fairly conventional and differ little from previously published models for excimer lasers, and we refer to Refs. 39–42 for representative listings of reactions and reaction rate coefficients. Our simulation differs from conventional models in two respects: in our treatment of high-gas-temperature plasma chemistry and in our accounting of the vibrational state densities of the XeF($C$) and XeF($B$) manifolds. Our treatment of high-gas-temperature plasma chemistry will be summarized in an upcoming publication. In our treatment of the vibrational manifolds, vibrational states within the XeF($C$) and XeF($X$) manifolds are assumed to be in thermal equilibrium, whereas we explicitly account for the vibrational states of XeF($B$). The model for vibrational exchange between XeF($B$) and XeF($C$) follows that of Lorents.[43] The rate constants for collisional exchange between the $B$ and $C$ manifolds used in our model are listed in Table II.

The excitation scheme for vibrational states of XeF($B$) is also modeled after that of Lorents,[43] who postulated that XeF($B$) is formed primarily in high vibrationally excited states. These states are lumped into a single "reservoir" state, XeF($R$), which represents XeF($B,v'$), $v' > 1$. The branching ratios for direct excitation of the vibrational levels of XeF($B$) used in the model are XeF($R$)/XeF($B,v1$)/XeF($B,v0$): 0.8/0.1/0.1. XeF($C$) is not directly populated in formation of excited XeF.

Gain is computed for the 351 and 353-nm $B \rightarrow X$ transitions by explicitly resolving the wavelength region 350–354 nm in a manner similar to that described by Blauer *et al.*[44] Densities of individual rotational levels of vibrational states were computed assuming the rotational distribution is in thermal equilibrium at the gas temperature. A representative emission spectrum is plotted in Fig. 5. The plasma-chemistry model was validated by comparing computed values of gain to the experimental results of Mandl and Hyman[45] for an $e$-beam pumped XeF laser. Good agreement was obtained, as shown in Fig. 6.

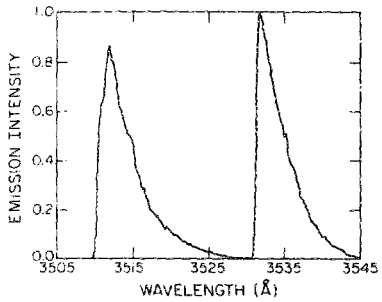


FIG. 5. Emission spectrum of XeF($B \rightarrow X$) computed with the plasma chemistry model for $e$-beam excitation of 3-atm $Ne/Xe/F_2 = 99.35/0.5/0.15$ at an average power deposition 135 kW cm$^{-3}$. The results are time averaged over a pump pulse of 1.3 $\mu$s.

## IV. COMPARISONS OF HEAVY-ION AND $e$-BEAM PUMPING

In this section, we make comparisons between heavy-ion excitation and electron-beam excitation of an XeF laser in a parameter space appropriate for fission-fragment excitation. The gas mixture is either $Ne/Xe/F_2$ or $Ne/Xe/NF_3$. The "standard" conditions are mole fractions of 98.85/0.773/0.377, pressure of 1.36 atm, peak pump power deposition of 2.4 kW/cm$^3$, and pump pulse width (FWHM) of

TABLE II. Reaction scheme for collisional mixing of vibrational manifolds of XeF($B,C$). For all excitation processes, the branching ratios for population of XeF* are XeF($R$)/XeF($B,v1$)/XeF($B,v0$) = 0.8/0.1/0.1. The vibrational states of XeF($C$) are assumed to be in thermal equilibrium. Rate constants are based on Ref. 43.

| Reaction | Forward rate[a] rate constant (cm$^3$ s$^{-1}$) | Reverse process activation energy (cm$^{-1}$) |
|---|---|---|
| XeF($R$) + Ne → XeF($B,v1$) + Ne | 2.50( − 12) | |
| XeF($R$) + Ne → XeF($C$) + Ne | 1.88( − 13) | |
| XeF($B,v1$) + Ne ⇄ XeF($C,v3$) + Ne | 6.25( − 13) | 75 |
| XeF($B,v1$) + Ne ⇄ XeF($B,v0$) + Ne | 4.00( − 11) | 443 |
| XeF($B,v0$) + Ne ⇄ XeF($C,v2$) + Ne | 1.30( − 12) | 123 |
| XeF($C,v0$) + Ne ⇄ XeF($C,v1$) + Ne | 3.00( − 12) | 614 |
| XeF($C,v3$) + Ne ⇄ XeF($B,v0$) + Ne | 6.25( − 13) | 368 |
| XeF($B,v1$) + $e$ ⇄ XeF($B,v0$) + $e$ | 1.00( − 7) | 443 |
| XeF($B,v0,v1$) + $e$ ⇄ XeF($C$) + $e$ | 1.00( − 7) | 0 |

[a] 1.0( − 10) ≡ 1.0 × 10$^{-10}$.

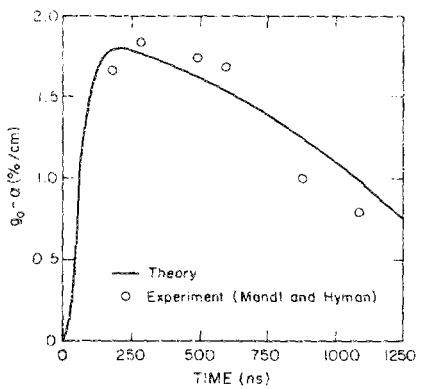


FIG. 6. Comparison of model results for net gain (gain − absorption) with experimental measurements of Mandl and Hyman (Ref. 45).

100 $\mu$s. In comparing fission-fragment to $e$-beam pumping, we use the same gas mixture and power deposition to allow the specifics of the pumping mechanism to be the only variable.

### A. Electron-product spectra

The product-electron spectrum, $\psi(\epsilon)$, for our standard conditions as produced by direct ionization by the fission fragments is compared to that produced directly by a 1-MeV $e$ beam in Fig. 7. Although both distributions peak at low energy, the $e$-beam-produced spectrum has a "tail" that reaches to energies exceeding a few keV, while that for the FF's does not exceed 1 keV. These results imply that a larger fraction of the energy of the $e$-beam electrons goes into the kinetic energy of product electrons compared to that of the FF's. The increment of energy transferred by the heavy ions to the orbital electrons is very near threshold. As a result, in an $e$-beam-pumped plasma the majority of the excitations and ionizations are performed by the product electrons and their secondary electrons due to their high ejection energy, and not the beam electrons. In contrast, in a heavy-ion-pumped plasma, there are as many excitations and ionizations caused directly by impact of the ions as by the product electrons. This is discussed further in Sec. IV C.

### B. Product-electron energy distribution

Using our standard conditions with $F_2$ the product-electron energy distribution function, $f(\epsilon)$, for a fission-fragment-generated plasma is compared to that generated by an $e$-beam in Fig. 8(a). The product-electron energy distribution function resembles the electron-product spectrum at energies much larger than the inelastic thresholds and above the energies for electron attachment. The distribution function for the $e$-beam-pumped plasma is relatively higher at high energy and depleted at low energy compared to that for the FF-generated plasma. At energies less than 10 eV, the attachment cross section is most influential for determining the shape of $f(\epsilon)$. The depletion of $f(\epsilon)$ at $\epsilon < 3$ eV is a result of rapid electron attachment. The mole fraction of the attaching gas and the details of the attachment cross section

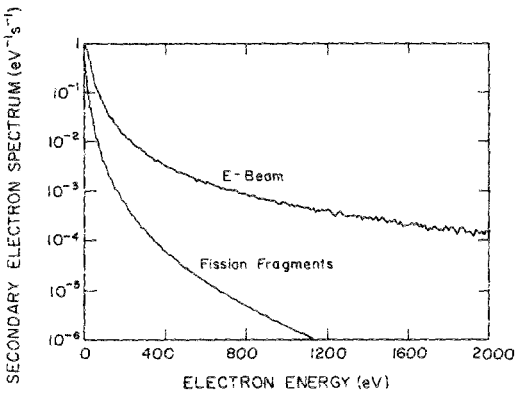


FIG. 7. Product-electron spectrum generated by the slowing of fission fragments and 1-MeV $e$ beam for our standard conditions normalized to unity at their maximum values. The $e$-beam-generated spectrum has a high-energy tail that exceeds 2 keV, whereas that produced by the heavy ions barely exceeds 1 keV.

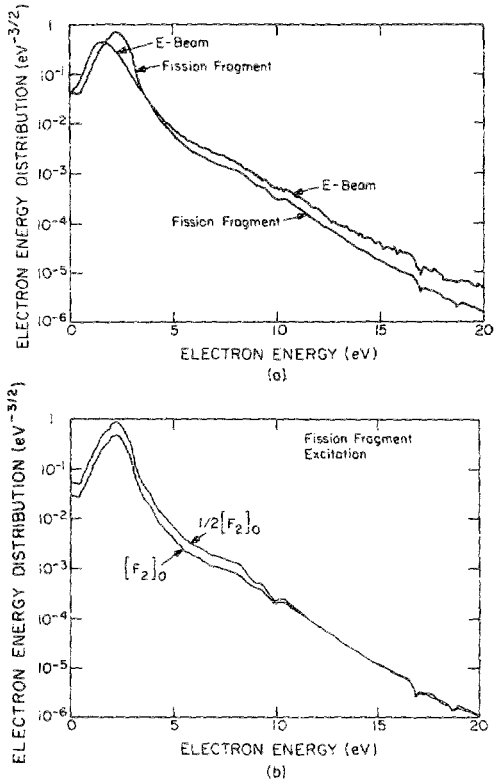


FIG. 8. Product-electron energy distributions for Ne/Xe/$F_2$ = 98.85/0.77/0.38 gas mixtures. (a) $e$-beam and fission-fragment excitation, (b) fission-fragment excitation with standard $F_2$ density and half the $F_2$ mole fraction.

have a large impact on the normalization of the distribution, and hence the absolute value of the resulting electron-impact rate constants, $k$ (cm$^3$ s$^{-1}$). There is little effect, though, on the absolute rate of excitation and ionization ($r = n_e N k$ cm$^{-3}$ s$^{-1}$) and hence $W$ values. This condition results from the fact that the attachment cross sections have little overlap with the excitation cross sections in this gas mixture and therefore do not affect the slowing of electrons from higher energies. Electrons attach only after having fallen below the ionization thresholds. This is further illustrated in Fig. 8(b) where the product-electron energy distribution in a FF-generated plasma is plotted for two different concentrations of $F_2$. Above 20 eV the distributions are essentially identical, but for electron energies in the range of the attachment cross section, the distribution with the lower $F_2$ concentration rises to a larger value. Because the attachment cross section continues to increase with decreasing energy, the average electron energy is fairly independent of the $F_2$ concentration. In gases where the attachment cross section is maximum at a nonzero energy, such as $NF_3$, $T_e$ increases as the attacher concentration increases, as discussed below.

The dependence of $T_e$ and selected rate coefficients on $NF_3$ fraction in a FF-generated plasma are plotted in Fig. 9(a). The variation of these values is important because of halogen burn-up which may occur during the FF or $e$-beam pumping pulse. Recall that the total rate of ionization, $n_e k_{ion} N = P/W$, is balanced by the rate of attachment, $n_e k_a [NF_3]$. As the $NF_3$ concentration decreases, $k_{ion}$ de-

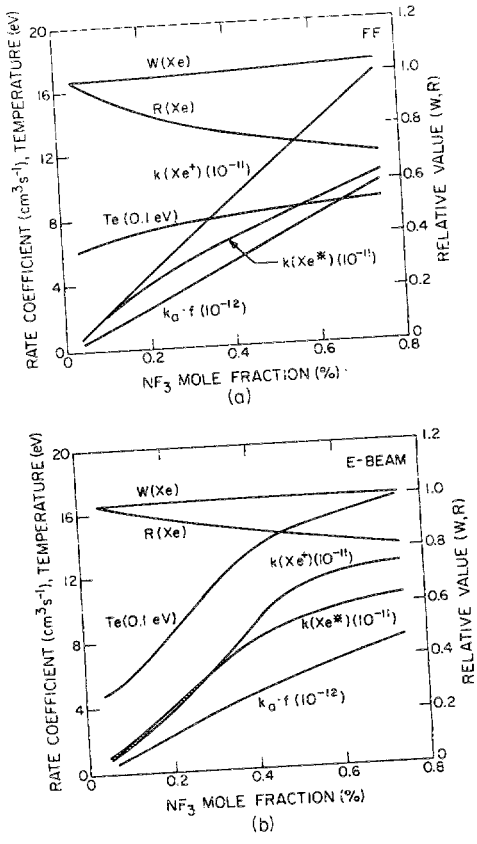


FIG. 9. Excitation parameters as a function of $NF_3$ mole fraction (Ne/Xe/$NF_3$ = 99.8/0.77/$X$) with (a) heavy-ion excitation and (b) $e$-beam excitation. The $W$ value and excitation fraction $R$ for xenon are given as relative values with the scale at right. Rate constants and electron temperature are given by the scale at left with exponent as noted.

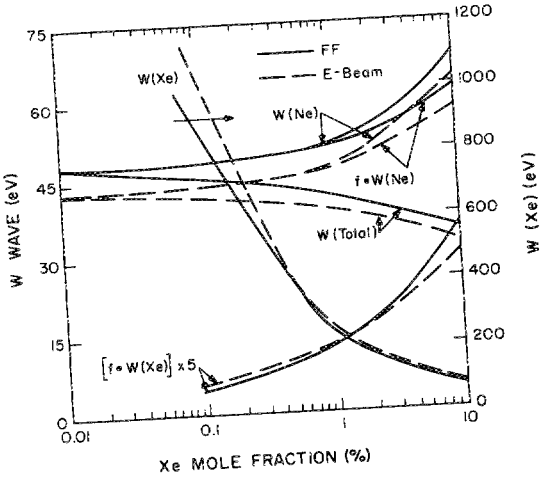


FIG. 10. Total, partial, and mole-fraction-weighted $W$ values for xenon and neon with FF and $e$-beam excitation as a function of xenon mole fraction. Note that the mole-fraction-weighted $W$ value for xenon has been multiplied by five for display purposes. $fW$(Xe) is less than the ionization potential of xenon at low xenon mole fraction because ionization is performed by electrons that fall below the ionization threshold of neon and would not be otherwise useful for ionization.

creases, and the electron density increases in such a manner to keep $n_e k_{ion}$ a constant and equal to $P/W$. The attachment rate coefficient we have plotted is weighted by the $NF_3$ mole fraction to emphasize the correlation with the ionization rate coefficient. The electron temperature increases with increasing $NF_3$ fraction, indicative of the loss of lower-energy electrons due to attachment. Note that the $W$ value for xenon is essentially constant, indicating that the rate of electron production is also nearly a constant in spite of the rate constant for ionization increasing. Although the excitation rate coefficient of xenon, as indicated by $k$(Xe*), increases with increasing $NF_3$, the absolute rate of excitation decreases, as indicated by $R$(Xe). This behavior results from some minor amount of competition between $NF_3$ and Xe near threshold for the excitation of Xe.

Rate coefficients and electron temperature for an $e$-beam-excited plasma appears in Fig. 9(b). The electron temperature is generally higher in the $e$-beam-pumped plasma. The linear relationship between the $NF_3$ fraction and ionization coefficient breaks down at high $NF_3$ fraction as a result of competition between $NF_3$ and the xenon ionization threshold.

$W$ values for FF- and $e$-beam-generated plamas are compared in Fig. 10 as a function of Xe mole fraction. The $W$ values are approximately 10% higher for FF excitation. This indicates that the high-energy $e$ beam and its secondary-electron spectrum are more efficient at ionizing these gas mixtures, a consequence of more efficient momentum transfer from the $e$ beam to orbital electrons, resulting in a more energetic secondary-electron spectrum. The total $W$ value decreases with increasing Xe mole fraction as more power is deposited in the more easily ionized Xe. The partial $W$ value for neon [$W$(Ne)] increases as the xenon mole fraction increases while that for xenon decreases [$W$(Xe)]. These trends are largely the result of the power deposition in a particular species scaling as its mole fraction. A better indication of the ionization efficiency is the mole-fraction-weighted $W$ value, $Wf$, as shown in Fig. 10. This value for xenon is much less than its ionization potential at low xenon mole fraction. Since the ionization potential for xenon is less than that for neon, electrons that fall below the ionization threshold of neon and no longer contribute to neon ionization can ionize xenon atoms. Therefore if the xenon mole fraction is low enough so that there is little competition between xenon and neon at higher energies, xenon is ionized by "waste electrons" falling below the neon threshold while not decreasing the rate of neon ionization. The incremental energy required to obtain an additional ionization of xenon is therefore small, if not zero.

Direct $W$ values for xenon and neon are plotted in Fig. 11. The ratio of direct to total $W$ value for $e$-beam excitation is $\approx$5–8, whereas that for FF excitation is $\approx$2–3. These ratios indicate that only 15%–20% of the ionization events in an $e$-beam-pumped plasma result directly from collisions with the beam electrons. The remainder are due to collisions with the product electrons. In a heavy-ion-pumped plasma, 30%–50% of all ionizations result from collisions directly by the heavy particles. This disparity is a result of the inability of the heavy ions to transfer significantly more energy than the ionization potential to the orbital electron. Therefore, the heavy ion slows by increments of energy not much greater than $u_i$ and expend most of their energy in this manner. In contrast, $e$-beam electrons efficiently transfer energy

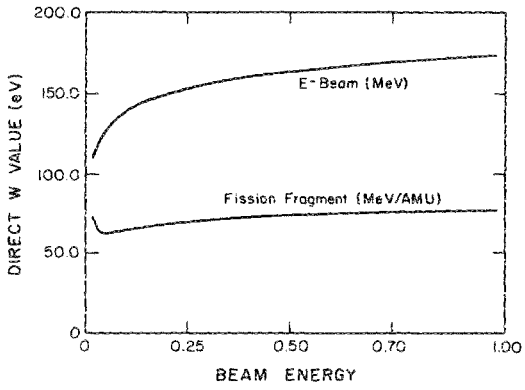


FIG. 11. Direct $W$ values (energy per ion pair produced directly by the beam projectiles) as a function of beam energy for electron-beam (MeV) and heavy-ion (MeV/amu) excitation. The larger value for $e$-beam excitation is a result of more kinetic energy being imparted to the secondary electron.

to the orbital electrons in increments that greatly exceed $u_i$. Therefore, fewer individual ionizations can be produced directly by the beam electrons for a similar amount of energy deposition. The difference between $W_D$ and the ionization potential is a measure of the average secondary electron and is larger for the $e$-beam-pumped system.

Excitation fractions, plotted in Fig. 12, display similar behavior as the $W$ values. At low xenon fraction $R(\mathrm{Xe})$ is large because excitations are produced by "waste" electrons that have slowed below the ionization thresholds of neon and xenon. Excitation does not compete with other processes and therefore proceeds efficiently. $R(\mathrm{total})$ is the $W$ value weighted sum of the $R$ values for neon and xenon. For FF pumping, $R(\mathrm{total})$ increases with increasing xenon mole fraction due to the larger fractional amount of power deposited in xenon, and the favorable match between the secondary-electron spectrum and the excitation cross sections of xenon. For $e$-beam pumping, $R(\mathrm{total})$ increases slightly and then decreases with increasing xenon mole fraction. This results from the ionization cross sections of xenon more effectively competing with excitation with the more energetic $e$-beam secondary-electron spectrum.

The total fractional excitation with FF pumping is larger than that with $e$-beam pumping; however, so is the $W$ value. The result is that the total number of excited states and ion pairs generated by the two pumping methods is not significantly different for moderate xenon mole fractions, as shown in Fig. 13. For xenon mole fractions less than 1%, $e$-beam excitation results in higher total excitation and ionization. Above 1%, more total excitation and ionizations are obtained by FF excitation. Unfortunately this is not an optimum parameter space for operation of an XeF laser due to quenching of the upper laser level by xenon and more absorption by $Xe_2^+$ and $NeXe^+$.

### C. $F_2$ vs $NF_3$ mixtures

The particular halogen donor, $NF_3$ or $F_2$, has a small impact on $W$ values and the net rate of ionization since the attachment cross sections for both species have little overlap with the excitation and ionization cross sections. Electron-impact rate coefficients, though, are different in the two mixtures due to differences in the attachment cross sections and resulting electron distribution functions. The electron distribution functions for gas mixtures containing $F_2$ and $NF_3$ are compared in Fig. 14. The cross section for dissociative attachment to $NF_3$ is maximum near 2 eV, which causes a depletion in $f(\epsilon)$ in that region. Since the cross section for attachment by $F_2$ is monotonically decreasing with increasing energy, the depletion occurs at lower energies. The distributions are nearly the same at energies at and above the excitation thresholds. The $NF_3$ attachment rate is larger relative to the excitation cross sections, and the depletion of intermediate-energy electrons effectively cools the distribution compared to the $F_2$ mixture, yielding a lower electron temperature, as shown in Table III. A higher electron temperature leads to a faster quenching of the precursor excited

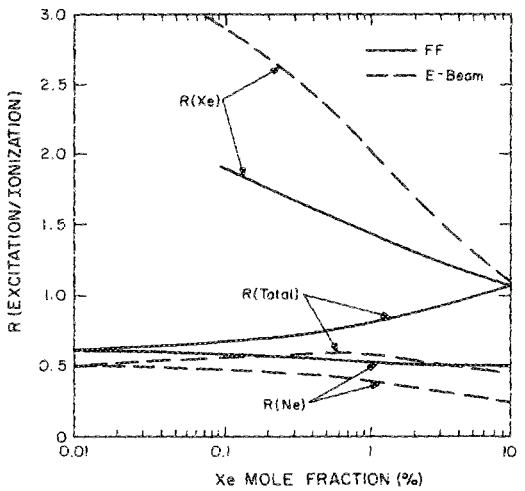


FIG. 12. Partial and total excitation fractions as a function of xenon mole fraction with FF and $e$-beam excitation. The total excitation fraction is maximum with $e$-beam excitation at approximately 1% xenon mole fraction, whereas that for FF excitation continues to increase.

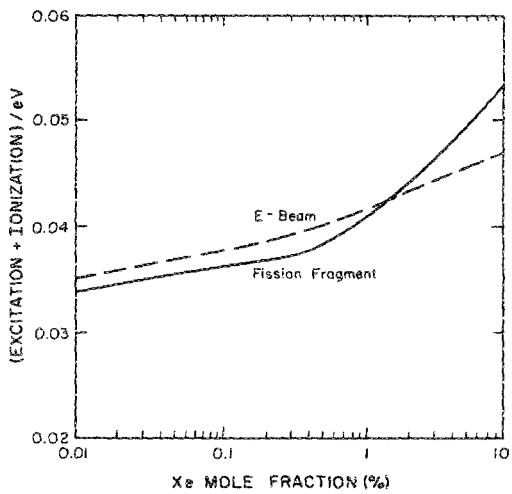


FIG. 13. Total number of excited states and ionizations per electron volt of deposited beam energy for fission fragments and $e$-beam excitation. Heavy-ion excitation actually results in more net excitation at high Xe mole fraction because of a favorable overlap of the beam-produced electron spectrum and the xenon excitation cross sections. Because of increased quenching and absorption, though, net laser gain is maximum at a lower xenon mole fraction.

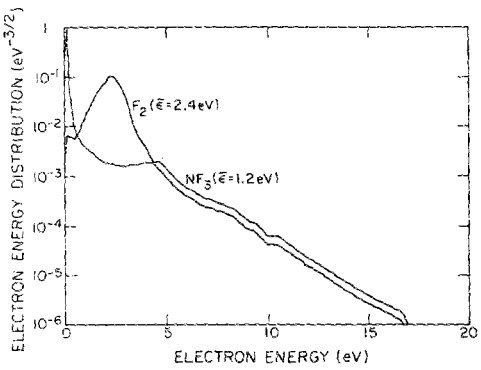


FIG. 14. Product-electron distribution functions for Ne/Xe/($F_2$,$NF_3$) gas mixtures with FF excitation. The average electron energies for the distributions are also shown.

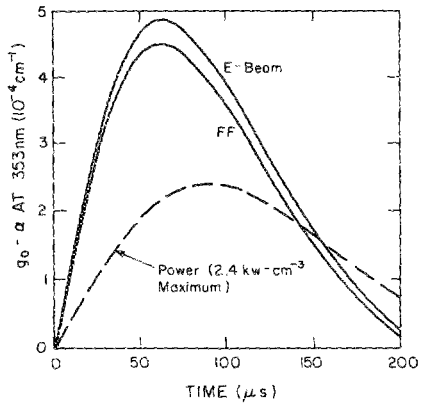


FIG. 15. Net small signal gain (gain − absorption) at 353 nm of XeF($B$) for our standard gas mixture with heavy-ion and $e$-beam excitation for conditions typical of FF excitation. Power deposition, also shown, has a maximum value of 2.4 kW cm$^{-3}$. $e$-beam excitation results in only moderately more gain.

states of XeF and reduces the rate of dissociative recombination, thereby increasing the relative dimer ion concentration.

In the $F_2$ gas mixture, the electron temperature is nearly the same for both pumping schemes. Since the attachment cross section is maximum at $\epsilon = 0$, all secondary electrons are created at energies above the peak. The electron temperature, which is determined by the energy at which the electrons attach to $F_2$, is therefore essentially the same for both systems. In the $NF_3$ mixtures, though, there is a sizable difference in $T_e$, as many of the electrons in the FF plasma are created below the peak in the $NF_3$ attachment cross section, thereby lowering the electron temperature compared to that for the $e$ beam.

## V. IMPLICATIONS OF EXCITATION OF XeF($B$)

The excitation and ionization rates discussed above were used as input to our plasma chemistry model to evaluate the efficiency of excitation of XeF($B$). In doing so we compare the relative merits of excitation by $e$-beam and heavy-ion sources. As an indicator of performance, we use the net small-signal gain, $g = g_0 - \alpha$, for the $B \rightarrow X$ transitions at 351 and 353 nm, where $g_0$ is the small-signal gain and $\alpha$ is the sum of the saturable and nonsaturable absorption.

The net small-signal gain for $e$-beam and FF excitation is shown in Fig. 15 for 2.4-kW cm$^{-3}$ peak power deposition. The $e$-beam-pumped plasma has $\approx 10\%$ more gain at 353 nm than with FF excitation using our standard conditions. The poorer performance with FF excitation is a result of the larger fraction of secondary electrons generated by heavy-ion ionization that appear below the excitation threshold compared to that for $e$-beam excitation, and the resulting increase in $W$ values. Given the uncertainties in our calculations, though, this decrease in performance is not terribly significant. The similar performance obtained with the two excitation methods is a consequence of the efficiency with which deposited power is channeled to the upper laser level in excimer laser systems (see below). The scaling of gain/(power deposition) we see here is comparable to that obtained with conventional $e$-beam excitation. Therefore, we appear not to pay a penalty for long-pulse, low-power deposition.

Note that the net gain is maximum prior to the peak in the pumping pulse. The energy deposition at peak power deposition is $\approx 265$ J/liter which results in an increase in gas temperature of $\approx 380$ K. The increase in gas temperature causes an increase in optical absorption by $NeXe^+$, whose absorption cross section increases with temperature.[44] It is well known, though, that XeF lasers show higher gain with moderate increases in the initial gas temperature (100–500 K above room temperature).[46] We also see this behavior for similar increases in gas temperature. It appears, then, that there is an optimum increase in gas temperature with respect to maximum gain in neon-based systems. The optimum is a tradeoff between a more favorable rotational vibrational distribution in the XeF($B$) manifold[46] and an increase in absorption from $NeXe^+$.

The parametric behavior of the gain versus gas mixture and power deposition is shown in Fig. 16. The ratio of net gain between $e$-beam and FF excitation is relatively constant over this parameter space. For our conditions, peak net gain is less than linearly proportional to power deposition. Part of

TABLE III. Pump parameters for Ne/Xe/($F_2$,$NF_3$) = 98.85/0.773/0.377.

| Halogen | Excitation system | $W$(Ne) (eV) | $W$(Xe) (eV) | $W_T$ (eV) | $R$(Ne) | $R$(Xe) | $T_e$ (eV) |
|---|---|---|---|---|---|---|---|
| $F_2$ | FF | 49.1 | 253.1 | 41.1 | 0.536 | 1.506 | 1.59 |
| | $e$-beam | 45.3 | 288.7 | 39.2 | 0.418 | 2.197 | 1.63 |
| $NF_3$ | FF | 50.3 | 269.1 | 42.4 | 0.542 | 1.503 | 0.794 |
| | $e$-beam | 45.3 | 288.1 | 39.2 | 0.420 | 2.177 | 1.338 |

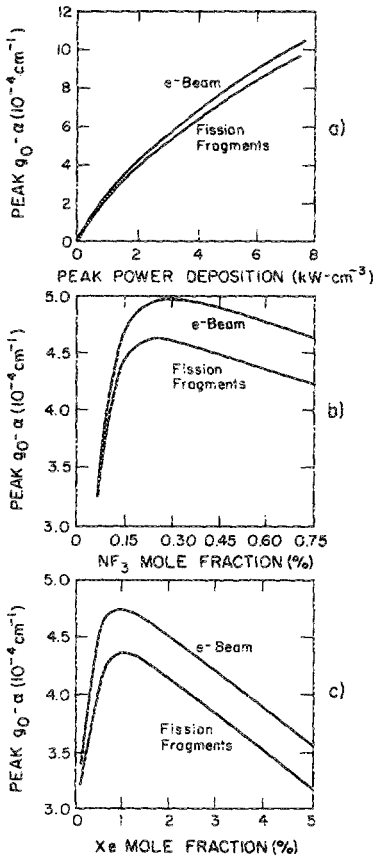


FIG. 16. Net small signal gain at 353 nm for fission-fragment and *e*-beam excitation of XeF($B$) as a function of (a) peak power deposition, (b) $NF_3$ mole fraction, and (c) Xe mole fraction.

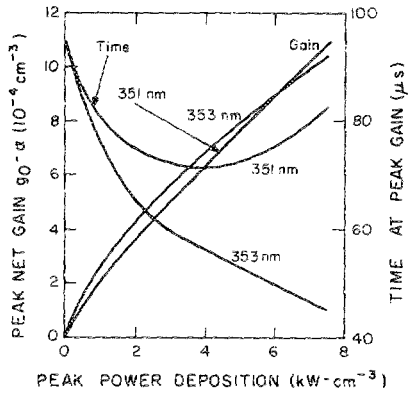


FIG. 17. Maximum net small signal gain at 351 and 353 nm for *e*-beam excitation of XeF($B$), and the time of maximum gain, as a function of power deposition. The peak power deposition occurs at $\simeq 95\,\mu$s.

the "roll-off" in net gain is a consequence of "burn-up" of $NF_3$. The $NF_3$ burn-up, though, is $<10\%$–$15\%$ due to its large reassociation constant and the long pumping time. The roll-off in peak net gain is largely due to increased absorption by $NeXe^+$ resulting from the higher gas temperature obtained with the higher power deposition.

Peak net gain is not particularly sensitive to $NF_3$ fraction, though gain peaks at a slightly higher fraction for *e*-beam excitation. Peak gain is more sensitive to xenon fraction, a consequence of a higher rate of quenching and larger fractional absorption by $Xe_2^+$.

At lower power deposition, maximum net gain is usually obtained at 353 nm. With increasing power deposition, though, maximum net gain is obtained at 351 nm, as shown in Fig. 17. The time at which net gain reaches its maximum value is a strong function of power deposition and temperature rise. Net gain at 353 nm peaks at earlier times compared to 351 nm as the power deposition, and hence gas temperature, increases. The time at which net gain at 351 nm is maximum remains close to the time of peak power deposition ($\simeq 95\,\mu$s). The relative amount of extractable energy at 351 nm should therefore increase with increasing power deposition.

## VI. CONCLUSIONS

We have developed a self-consistent method to analyze the pumping of excimer lasers by fission fragments and have compared the pumping mechanisms to electron-beam-excited systems. A comparison of laser performance proceeded by independently obtaining excitation and ionization rates and using them as input to the same plasma-chemistry model for an XeF laser. The higher threshold energy events that weakly compete with attachment by the halogen donor are represented by the energy per ionization, $W$, and the number of excitations per ionization, $R$.

We found that the fission fragments, due to their large mass, transfer less energy per collision to orbital electrons than do the *e*-beam electrons. As a result, with fission-fragment pumping the secondary product electrons have, on the average, enough energy for only a single additional ionization. With *e*-beam excitation, the product electrons have enough energy to ionize five to ten times. The total $W$ value with fission-fragment pumping was found to be 10% higher than for *e*-beam pumping while the electronic excitations per ionization are higher with FF excitation. These results imply that more of the *e*-beam energy goes into ionization, whereas the fission fragments favor electronic excitations in pure rare gases. The total number of excitations and ionizations are generally higher for *e*-beam excitation at low to moderate xenon fractions. At high xenon fractions, more excitations are obtained with FF excitation, though in a parameter space that is not optimum for generating high net gain in an XeF($B \rightarrow X$) laser.

Within the uncertainties of our calculations, there appears to be no significant disadvantage to heavy-ion excitation of excimer lasers, as the decrease in net gain is only 10%–15% compared to *e*-beam pumping. Although the details of the excitation processes differ due to differences in the momentum transfer between projectile and target, the high efficiency with which deposited energy "flows" to the upper laser level through either the neutral or ion channels in excimer laser systems[47] tends to blur these differences. The equivalent performance of the pumping methods will likely not hold for systems which rely solely on either a neutral or ion-pumping channel. The advantage, then, of fission-fragment excitation of excimer lasers lies in the availability of long pump pulses and high-total-energy deposition that are not possible with conventional *e*-beam pumping.

## ACKNOWLEDGMENTS

The authors thank Dr. G. N. Hays, Dr. J. B. Gerardo, Dr. J. K. Rice, and Dr. D. MacArthur of Sandia National Laboratories for helpful discussions and guidance. This work was supported by the Department of Energy, Sandia National Laboratory, Albuquerque.

## APPENDIX: SPECTRUM OF FISSION FRAGMENTS INCIDENT ON THE LASER GAS MIXTURE

In this appendix, the procedure for computing the energy spectrum of fission fragments, $\varphi(\epsilon)$, incident on the gas mixture in the laser cavity will be described. The fraction of trajectories of fission fragments from depth $x$ below the surface of the foil that reach the surface with the length of the trajectory being less than $\rho$, is given by

$$P(\rho,x)=\frac{1}{4\pi}\int_{\cos\theta_0}^{1} d\Omega=\tfrac{1}{2}(1-\cos\theta_0)=\tfrac{1}{2}\left(1-\frac{x}{\rho}\right), \tag{A1}$$

where $\theta_0$ is the angle of the trajectory from the vertical. The probability of a trajectory having a specific length $r$ is

$$p(r,x)=\left.\frac{dP(\rho,x)}{dr}\right|_{\rho=r}=\frac{x}{2r}. \tag{A2}$$

Integrating over all positions $x$ gives the spectrum of trajectories reaching the surface having length $r$,

$$\xi(r)=\int_0^{x_{\max}} dx\, p(r,x)=\frac{x_{\max}^2}{4r^2}$$
$$=\begin{cases}0.25, & r<T\\ T^2/4r^2, & r>T\end{cases} \tag{A3}$$

where $T$ is the thickness of the foil. $R(\epsilon)$ is the range of a fission fragment with energy $\epsilon$, so the trajectories are of length $r(\epsilon)=R(\epsilon_0)-R(\epsilon)$, where $\epsilon_0$ is the initial fission-fragment energy. These trajectories are related to the fission-fragment spectrum by

$$\varphi(\epsilon)=\xi(r)\left|\frac{dr}{d\epsilon}\right|$$
$$=\begin{cases}\partial R/\partial\epsilon, & \epsilon>\epsilon^*,\\ T^2/[R(\epsilon_0)-R(\epsilon)]^2, & \epsilon<\epsilon^*,\end{cases} \tag{A4}$$

where $\epsilon^*$ is the energy corresponding to the difference in range between that of the initial energy and the thickness of the foil, $R(\epsilon^*)=R(\epsilon_0)-T$. It is usual to use a four-parameter fit to relate energy to range by

$$\epsilon(R)=aR^b+cR^d \Rightarrow \frac{\partial\epsilon}{\partial R}=abR^{b-1}+cdR^{d-1}, \tag{A5}$$

$$\epsilon^*=a[R(\epsilon_0)-T]^b+c[R(\epsilon_0)-T]^d. \tag{A6}$$

Given these quantities, the fission-fragment spectrum, $\varphi(\epsilon)$ can be computed. We find it more convenient to work in terms of velocity rather than energy, and convert to velocity by

$$\varphi(V)=\varphi(\epsilon)\frac{\partial\epsilon}{\partial V}=MV\varphi(\epsilon). \tag{A7}$$

where $M$ is the mass of the projectile. The total power flux of fission fragments into the gas mixture is the sum of contributions from the light and heavy fragments of $^{235}$U.

[1]J. J. Ewing, in *Laser Handbook* (North-Holland, New York, 1979), Vol. 3, pp. 135–197.
[2]Ch. A. Brau, *Excimer Lasers*, 2nd ed., edited by C. K. Rhodes (Springer Verlag, Berlin, 1984), pp. 87–137.
[3]R. A. Hass, *Gas Lasers*, Vol. 3 of *Applied Atomic Collisions Physics*, edited by E. W. McDaniel and W. L. Nighan (Academic, New York, 1982), pp. 423–452.
[4]K. Thom and R. T. Schneider, AIAA J. **10**, 400 (1972).
[5]R. J. DeYoung, N. W. Jalufka, and F. Hohl, AIAA J. **16**, 991 (1978).
[6]R. J. DeYoung, Appl. Phys. Lett. **38**, 297 (1981).
[7]A. M. Voinov, L. E. Dovbysh, V. N. Krivonosov, S. P. Mell'nikov, I. V. Podmoshenskii, and A. A. Sinyanskii, Sov. Tech. Phys. Lett. **7**, 437 (1981).
[8]D. A. McArthur and P. B. Tollefsrud, Appl. Phys. Lett. **26**, 187 (1975).
[9]H. H. Helmick, J. Fuller, and R. T. Schneider, Appl. Phys. Lett. **26**, 327 (1975).
[10]R. J. DeYoung, N. W. Jalufka, and F. Hohl, Appl. Phys. Lett. **30**, 19 (1977).
[11]A. M. Voinov, L. E. Dovbysh, V. N. Krivonosov, S. P. Mel'nikov, I. V. Podmoshenskii, and A. A. Sinyanskii, Sov. Phys. Tech. Phys. **27**, 819 (1982).
[12]G. A. Batyrbekov, S. A. Kostritsa, Yu. E. Kuz'min, A. B. Tleuzhanov, and M. U. Khasenov, Sov. Phys. Tech. Phys. **8**, 341 (1982).
[13]R. J. DeYoung and W. R. Weaver, J. Opt. Soc. Am. **70**, 500 (1980).
[14]H. Elsayed-Ali and G. Miley, in *Proceedings of the International Conference on Lasers '83*, edited by C. B. Collins (STS, McLean, VA, 1984), pp. 401–405.
[15]J. W. Wilson, Appl. Phys. Lett. **37**, 695 (1980).
[16]J. W. Wilson and A. Shapiro, J. Appl. Phys. **51**, 2387 (1980).
[17]S. J. S. Nagalingham and G. Miley, in *Proceedings of the International Conference on Lasers '80*, edited by C. B. Collins (STS, McLean, VA, 1981), pp. 699–707.
[18]B. D. Carter, M. J. Rowe, and R. T. Schneider, Appl. Phys. Lett. **36**, 115 (1980).
[19]A. I. Mis'kevich, A. B. Dmitriev, V. S. Il'yashchenko, B. S. Salamakha, V. A. Stepanov, and E. M. Gorodkov, Sov. Tech. Phys. Lett. **6**, 352 (1980).
[20]G. N. Hays, D. A. McArthur, D. R. Neal, and J. K. Rice, Appl. Phys. Lett. **49**, 363 (1986).
[21]T. Moratz and M. J. Kushner, J. Appl. Phys. **63**, 1796 (1988).
[22]G. H. Miley and P. E. Theiss, Nucl. Appl. **6**, 434 (1969).
[23]J. C. Guyot, G. H. Miley, and J. T. Verdeyen, Nucl. Sci. Eng. **48**, 373 (1972).
[24]D. H. Nguyen and L. M. Grossman, Nucl. Sci. Eng. **30**, 233 (1967).
[25]B. K. Srivastava and S. Mukherji, Phys. Rev. A **14**, 718 (1976).
[26]H. Betz, Rev. Mod. Phys. **44**, 465 (1972).
[27]M. Gryzinski, Phys. Rev. **138**, 336 (1965).
[28]H. A. Hassan and J. E. Deese, Phys. Fluids **19**, 2005 (1974).
[29]R. H. Lo and G. H. Miley, IEEE Trans. Plasma Sci. **PS-2**, 198 (1974).
[30]S. Yoshida, A. V. Phelps, and L. C. Pitchford, Phys. Rev. A **27**, 2858 (1983).
[31]C. B. Opal, W. K. Peterson, and E. C. Beaty, J. Chem. Phys. **55**, 4100 (1971).
[32]K. Tachibana and A. V. Phelps, Phys. Rev. A **36**, 999 (1987).
[33]D. Rapp and P. Englander-Golden, J. Chem. Phys. **43**, 1464 (1965).
[34]M. Hayashi, J. Phys. D **16**, 581 (1983).
[35]N. J. Mason and W. R. Newell, J. Phys. B **20**, 1357 (1987).
[36]M. Hayashi and T. Nimura, J. Appl. Phys. **54**, 4879 (1983).
[37]P. J. Chantry, in *Gas Lasers*, in Vol. 3 of *Applied Atomic Collisions Physics*, edited by E. W. McDaniel and W. L. Nighan (Academic, New York, 1982), pp. 35–70.
[38]T. J. Moratz, L. C. Pitchford, and J. N. Bardsley, J. Appl. Phys. **61**, 2146 (1987).
[39]H. Hokazono, K. Midorikawa, M. Obara, and T. Fujioka, J. Appl. Phys. **56**, 680 (1984).
[40]R. Sauerbrey, W. Walter, F. K. Tittel, and W. L. Wilson, J. Chem. Phys. **78**, 735 (1983).
[41]M. Ohwa and M. Obara, J. Appl. Phys. **59**, 32 (1986).
[42]F. Kannari, M. Obara, and T. Fujioka, J. Appl. Phys. **57**, 4309 (1985).
[43]D. C. Lorents, SRI International Research Report No. MP 83-142 (1983).
[44]J. A. Blauer, T. T. Yang, C. E. Turner, and D. A. Copeland, Appl. Opt. **23**, 4352 (1984).
[45]A. E. Mandl and H. A. Hyman, IEEE J. Quant. Electron. **QE-22**, 349 (1986).
[46]D. H. Burde, T. T. Yang, D. G. Harris, L. A. Pugh, H. H. Tillotson, C. E. Turner, and G. A. Merry, Appl. Opt. **26**, 2539 (1987).
[47]M. J. Kushner, Bull. Am. Phys. Soc. **32**, 1174 (1987).